Comparative Analysis of Pulsatile and Steady Flow on Arterial Mass Transport

S.A. Gabriel[1], Y. Ding[1], Y. Feng[2] and J.A. Gear[1]

[1]School of Mathematical and Geospatial Sciences
RMIT University, Melbourne, Victoria 3001, Australia

[2]Mineral Resources Flagship
CSIRO, Clayton, Victoria 3169, Australia

Abstract

Blood flow in the cardiovascular system operates on a periodically-repeating time scale which influences flow-driven mass transport. For this reason, it is difficult to model physiological phenomena that have characteristic time scales larger than that of a pulse period. In attempt to overcome this limitation for mass transport, this study looks at reducing flow variations within a time period to a characteristic flow profile, via time averaging over the whole period. A computational model is developed to capture transient physiological flow physics, and incrementally record the flow-field for time-averaging. The calculated time-averaged flow profile, which represents the effective convective velocity in a time period, is then used as a convective vector field for scalar transport. It is shown that the time-averaged flow-field is inappropriate for deriving other flow variables such as wall shear stress, but may be used for transport purposes as a convective profile.

Introduction

The cardiovascular system is a circulatory transport system for blood, which carries nutrients, wastes and other materials to and from tissues throughout the body. The system is predominantly driven by the heart, which creates pressure differentials to drive blood flow. Physiological blood flow characteristically varies temporally and operates in a periodic manner due to the rhythmic contractions of the heart. Flow transport is therefore irregular on a continuous monotonic time scale.

This makes it difficult to assess the evolution of physiological phenomena that operate on long time scales, but are also influenced by the short periodic time scales of the flow. Mass transport is such a phenomenon that is both an important process to the function of the cardiovascular system and is integral to the genesis and development of cardiovascular diseases such as atherosclerosis and thrombosis. Concerning atherosclerosis, the transport of low density lipoprotein (LDL) macromolecules from the lumen to the surrounding arterial wall plays an essential role in the inflammatory responses to the disease, particularly at regions with abnormally elevated concentrations of LDL.

Experimental studies have established that wall shear stress (WSS) induced by dynamic blood flow, plays an important role in the regulation of LDL flux from the lumen into the arterial wall [9]. Analogous computational models have also been shown to confirm such findings [12, 13]; however these studies often neglected important characteristics of physiological flows, particularly the temporal nature of the working fluid. The reason for this omission is noted to be primarily due to the difficulty in modelling both short and long time scales for many time periods; because of the large difference in characteristic sizes of the two time scales involved, a complete resolution of both time scales would be prohibitively expensive on computational resources.

Consequently, developments of complex models associated with the cardiovascular system have been in part hindered or else simplified by this limitation. It is the intent of this study to overcome this limitation by identifying methods to unify both time scales into a single continuous scale. One such approach involves averaging flow-field variables over a characteristic time period [7]. The purpose for this being that temporally varying variables reduce to single values. In the field of cardiovascular flow modelling, this approach is popularly applied to obtain time-averaged statistics of WSS and residence times of flow-transported scalars [1, 6, 8, 15].

Whilst the above approach is satisfactory for flows that reach periodically repeating behaviour within a few time periods from arbitrary initial conditions (generally 3-4 periods for blood flow in moderately complex arterial geometries), it may not be so if there are extra physics applied to the model. This is true for flow-transported scalars with high Peclet numbers and complex boundary conditions, where a lot more time periods may be required before the solution takes a periodically repeating state. In the case of modelling atherosclerosis, this becomes particularly important for scalar transport at near-wall regions, where most of the significant physics takes place.

Since the temporal flow-field is known to converge to a periodically repeating state with reasonably few iterations, this study attempts to work with the stabilized period flow-field to derive the other variables of interest. For practicality of use, particularly in the modelling of atherosclerosis where the time scale of interest is orders of magnitude larger than the periodic time scale, it is useful to combine both time scales into a single continuous variable. To do this, time averaging of the whole flow-field rather than derived variables is performed. The averaged flow-field can thus be treated as a fixed velocity profile and used for other physics such as scalar transport. In doing so, integer multiples of a single period length can be made to represent a unit of time on the average flow-field.

Model Setup

Geometry

Bifurcating arterial geometries are noted to contain disturbed flow regions in both steady and unsteady conditions. These disturbances are commonly found at the flanks of the bifurcating site (refer to figure 1), and are generally wall-attached recirculation zones. It is known that the size of the recirculation zone varies within a given period, indicating that the walls they attach to experience low and oscillatory shear stress; both of these being important parameters in the formation of atherosclerosis [9, 11]. As this study is concerned with evaluating the appropriateness of time-averaged flow in cardiovascular modelling, it is seen fit by the authors to set it in the context of flows that are used for atherosclerosis modelling. Therefore, for the purpose of investigating time-averaged resolution of such

disturbances, a simplified 2-dimensional arterial bifurcation is selected for this study. The geometry is the same as that presented in [4], and is the 2-dimensional channel section found at the symmetry plane of a symmetric bifurcation; its dimensions are provided in figure 1. The geometry comprises of the bifurcation site, which is the region of interest for this study, particularly at the outer walls of the bifurcation. Flow extensions are also included both upstream and downstream of the region of interest, so that it is minimally affected by the inlet and outlet boundary conditions. This is particularly important for simulations involving transient physiological flow, which may cause for reverse flow regions to emerge.
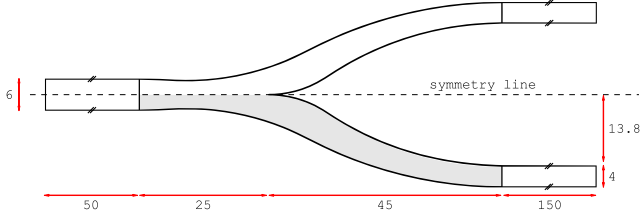

Figure 1. Computational domain of interest geometry (shaded region); flow extensions added upstream and downstream; units in [*mm*].

Governing Equations

If the geometry presents no significant disturbances to the flow-field, then within medium-sized arteries at typical physiological conditions, flow is predominantly laminar. Therefore, to describe arterial blood flow, the unsteady incompressible mass and momentum (Navier–Stokes) continuity equations are employed. These equations are given by:

$$\nabla \cdot \boldsymbol{u} = 0 \tag{1}$$

$$\rho \partial_t \boldsymbol{u} + \rho(\boldsymbol{u} \cdot \nabla)\boldsymbol{u} - \mu \nabla^2 \boldsymbol{u} + \nabla p = 0 \tag{2}$$

Where the velocity and pressure fields are denoted by $\boldsymbol{u}$ and p respectively. The working fluid is assumed to be homogenous with isotropic properties characteristic of blood in medium-large arteries; density is given by $\rho = 1050 \, kg/m^3$ and viscosity by the Newtonian approximation of $= 3.05 \times 10^{-3} \, kg/m/s$ [2].

Scalar transport is implemented using an unsteady convection-diffusion equation. For, the unsteady scalar transport equation for a scalar concentration c is given by:

$$\partial_t c + \boldsymbol{u} \cdot \nabla c - D\nabla^2 c = 0 \tag{3}$$

Where $\boldsymbol{u}$ is a divergence-free vector field and D is a constant isotropic diffusivity. For this study, the scalar is set to represent LDL concentration within blood flow, therefore a typical diffusion coefficient of $D = 5.0 \times 10^{-12} \, m^2/s$ is assigned [2].
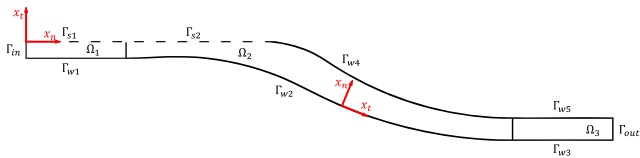

Figure 2. Labels of boundaries Γ_i and domains Ω_i for geometry (where i is an index). Local boundary coordinate systems are denoted by the surface normal axis x_n and tangential axis x_t.

At the flow inlet boundary Γ_{in}, the scalar is assigned a uniform Dirichlet condition $c = 1$ and the flow velocity normal to the boundary is assigned a scaled Poiseuille velocity profile u_n:

$$u_n = 2 f_s u_{av} \left(1 - 4\left(\frac{x_t}{d}\right)^2\right) \tag{4}$$

Where d is the arterial inlet diameter, f_s is a scaling factor and u_{av} is the average flow velocity at inlet, derived from the bulk flow Reynolds number:

$$Re = \rho u_{av} d / \mu \tag{5}$$

The scaling factor f_s is defined as a function of time, such that its time-average over one period is $\overline{f_s} = 1$. The temporal profile of f_s is derived from [5] and is provided in figure 3. In steady-state, the scaling factor takes its time-averaged value $f_s = \overline{f_s}$ and equation (4) becomes a standard Poiseuille velocity profile.
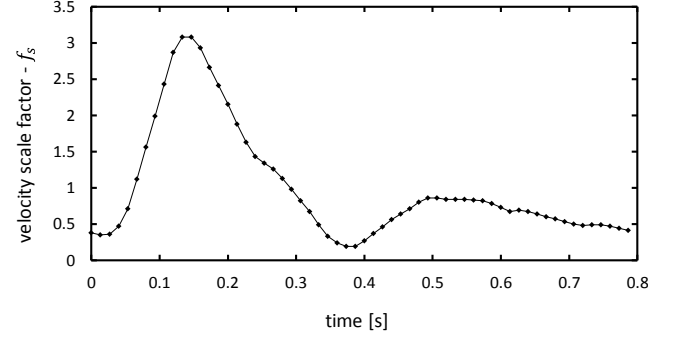

Figure 3. Physiological flow scaling factor variation in one period.

At the flow outlet boundary Γ_{out}, a zero-flux Neumann condition is assigned to the scalar transport equation. This condition is unrealistic as it forces a fully-developed state on the growing scalar transport boundary layer. However, due to the inclusion of flow extensions at the outlet, it is not expected that this condition would affect the scalar transport in the domain of interest Ω_2, and so is safe to use.

At the boundaries Γ_{si} on the symmetry plane, symmetry conditions are assigned to both flow and scalar transport equations. The remaining Γ_{wi} boundaries are walls, and so are assigned with no-slip wall conditions in the flow equations. For the scalar transport equation, the boundary conditions are not the same for all Γ_{wi}. At the wall boundaries Γ_{w1}, Γ_{w4} and Γ_{w5}, a scalar transport boundary layer is of no interest to this study, so a Dirichlet condition of $c = 1$ is assigned to prevent its formation. At the wall of interest Γ_{w2} and its downstream wall Γ_{w3}, scalar flux into the arterial wall is modelled as the sum of convective flux (due to water infiltration velocity V_w) into the boundary and diffusive flux away from the boundary [3]; this is given by:

$$K c_w = V_w c_w - D \frac{\partial c}{\partial x_n} \tag{6}$$

Where c_w is the scalar concentration at the boundary and K is the endothelial wall's permeability coefficient to the scalar. Water infiltration velocity is set to the generally accepted constant value of $V_w = 1.78 \times 10^{-8} \, m/s$ [10]. The scalar's wall permeability coefficient is set to that of what would be expected of LDL permeability, and is assigned a WSS τ_w dependance. Following the results of Himburg et al. [5], the permeability coefficient is scaled to take the vale $K_0 = 2.0 \times 10^{-10} \, m/s$ at undisturbed flow regions [14], where the undisturbed flow WSS magnitude $|\tau_{w0}|$ is approximated by the Poiseuille flow result:

$$|\tau_{w0}| = \frac{8\mu^2}{\rho d^2} Re \tag{7}$$

The resulting description of the permeability coefficient is given by the power law correlation:

$$K = K_0 \left(\frac{|\tau_{w0}|}{|\tau_w|}\right)^{0.118} \tag{8}$$

Model Description

The governing equations and associated boundary conditions are assigned to the volumetric domains Ω_i and enclosing boundaries Γ_i respectively (refer to figure 2). In this study, the model is

implemented and solved using the unstructured finite volume solver ANSYS Fluent v14.5.

For this study, three modelling cases are assessed:

1. Steady-state flow and scalar transport
2. Time-averaged flow and scalar transport
3. Time-averaged flow and steady-state scalar transport

In case 1, all equations for a given Reynolds number are solved to steady-state (unsteady terms in equations (2) and (3) are set to zero and $f_s = 1$). In case 2, all equations are solved in transient form for at least N periods; where N is defined as the minimum number of periods required for the flow to stabilize periodically. At period N, the flow-field and scalar distribution (and other variables of interest) are time-averaged over the length of the period, as denoted by equation (9) for the generic variable ϕ.

$$\bar{\phi} = \frac{1}{T}\int_{t_0}^{t_0+T} \phi\, dt \approx \frac{1}{T}\sum_i \phi_i \Delta t_i \qquad (9)$$

The time-averaged flow-field in case 2 is then used to drive the scalar transport in case 3; for this analysis it is solved to steady-state. The purpose of this case being that the time-averaged flow-field represents convective transport of the scalar variable over the length of a whole period.

Results and Discussion

The present study is made for physiological flow conditions, therefore a Reynolds number $Re = 500$, typical of medium-large sized arteries, is considered. Since solutions are expected to be Reynolds number dependant, to generalize results to neighbouring Reynolds numbers, the following dimensionless parameters are defined:

$$u^* = \frac{|\boldsymbol{u}|}{u_{av}} \quad, \qquad \tau_w^* = \frac{\tau_w}{\frac{1}{2}\rho u_{av}^2} \qquad (10)$$

For this setup, convergence of the case 2 unsteady flow-field was achieved by the third period. Using this converged periodic state, a comparison of the luminal flow velocity profile for the steady-state and time-averaged flow is given in figure 4. Both flow-fields are noted to display similar behaviour at regions of undisturbed flow (e.g. location 1 in figure 4). However, at the bifurcation site, particularly at the recirculation zone, variations in the flow-field are distinct (locations 2 and 3).
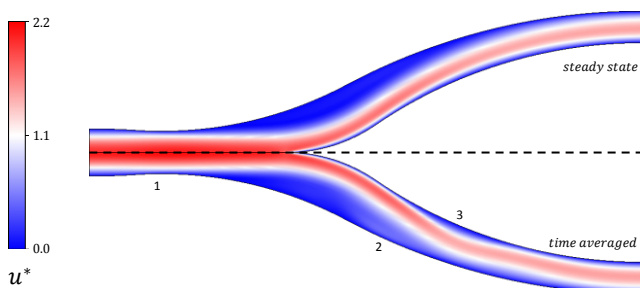

Figure 4. Comparison between steady-state and time-averaged luminal flow velocity distribution.

In time-averaged flow, the recirculation zone is notably smaller in length, with higher velocity at its downstream end (i.e. at location 2); indicating that its length varies throughout a time period. The presence of high velocity in the recirculation zone is a result of signed velocity vector averaging over the time period (refer to equation (9)) and not due to a physical manifestation of the flow-field; it is therefore physically unrealistic and may lead to inaccurately derived flow variables. An example is given by the unrealistic spike in WSS derived from the time-averaged flow

(figure 5, case 3, position 0.6). This indicates that derived flow variables of the time-averaged flow-field would be inappropriate representations of their actual values. The purpose of the time-averaged flow-field is therefore not to derive other flow variables, but rather to give a single time-independent representation of convective transport of the flow in a period. Flow variables of interest should therefore be explicitly solved for via time-averaging from the temporal flow-field; for example, the WSS calculated in case 2 (figure 5).
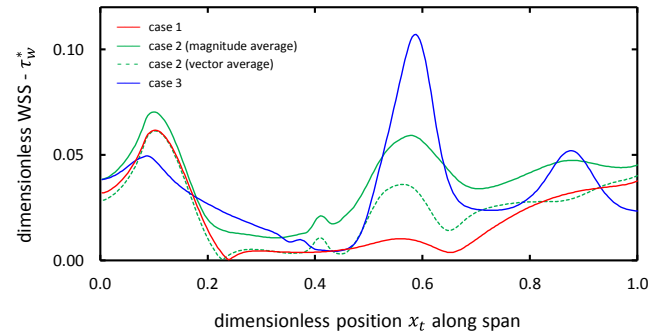

Figure 5. Wall shear stress along span of Γ_{w2}.

Furthermore, since the flow velocity is a vector quantity, then at locations where the signed flow direction varies, the time-averaging of derived vector variables will differ from that of their magnitude. This is illustrated by the WSS of case 2 in figure 5, where the magnitude average is always greater or equal to that of the vector average. The vector average WSS is noted to closely resemble that of the steady-state case at regions of undisturbed flow; i.e. where the flow was little affected by the recirculation zone. However, within the recirculation zone, particularly towards the downstream end, there is a marked difference which corresponds to the temporal variation in size of the recirculation zone during a period.

For this reason, depending on the requirements from time-averaged vector variables, either formulation may be of importance. In the case of atherosclerosis modelling, if mass transfer at a wall is modelled as a function of WSS magnitude, then the time-averaged WSS magnitude statistic would be required alone. If a measure of oscillation is also required, then both time-averaged WSS vector and magnitude statistics would be important. The difference between both statistics provides a measure for WSS direction variation in a period; such that a zero difference would imply WSS with no signed direction change.

Referring back to figure 4, another location of flow variation is noted at location 3, where an apparent recirculation zone is found attached to Γ_{w4}. However, the local time-averaged flow-field does not display reverse flow, but rather a low-velocity zone with no signed direction change. This indicates that the temporal flow has a short-lived recirculation zone within a period. The presence of this recirculation zone, though short-lived, will influence the process of mass transport into the arterial wall. That this short-lived recirculation zone was not revealed by the steady-state flow indicates the importance of resolving unsteady flow for better capture of WSS and thus mass transport into the arterial wall.

Whilst providing a useful measure of the temporal flow-field, time-averaged flow, as described in this paper, has thus far found very little use in the study of cardiovascular flows. A potential application is investigated in this paper, where scalar transport is studied under the convective influence of a time-averaged flow-field. A summary of results for the scalar described earlier is given by a plot of concentration distribution on Γ_{w2} (figure 6). As denoted by the plot for case 2, scalar transport did not reach periodic repeatability within the five periods tested; where five periods are regarded as computationally excessive for tasks

involving multiple iterations of this process. For this reason, making use of time-averaged flow to describe the convective behaviour of a period is especially useful.
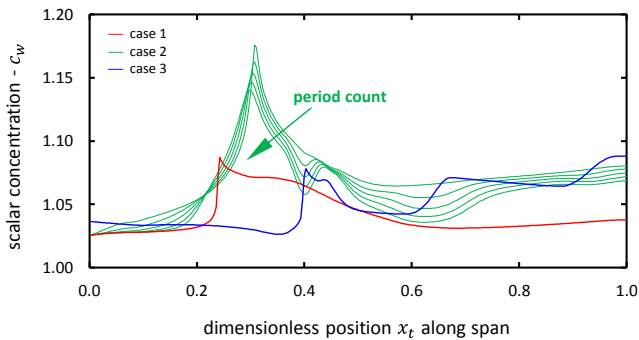

Figure 6. Scalar concentration along span of Γ_{w2}.

From the scalar distribution plot, it is noted that all three cases display similar results in the upstream regions; where flow is little disturbed. However, judging from the apparent convergence of the case 2 scalar profile, two distinctive peaks are noted (at positions 0.3 and 0.45). The larger peak appears to correspond to the peak of the steady state profile of case 1 and the smaller to that of case 3 (derived from the time-averaged flow-field). At the downstream end (i.e. aft of position 0.5), the case 2 scalar profile is better represented by that of case 3. However, as the case 2 plot did not converge, these results are not conclusive.

An overall assessment of the plot reveals no significant relationship between either of the three case studies investigated. As such, the effectiveness of the time-averaged flow field in convecting scalar transport cannot be conclusively commented upon from these results. Further studies are required to verify this; particularly the final convergence state of the case 2 scalar profile for appropriate comparison to the other cases.

Conclusions

This study investigates time-averaged flow of a periodic flow profile for the purpose of representing convective transport in a period. With applications in cardiovascular flow modelling of mass transport, this study also investigates time-averaged flow influence on scalar transport. A computational model is developed, and flows under steady-state and time-averaged regimes are comparatively investigated. It is revealed that a steady-state flow will not resolve all features of an unsteady flow, particularly those that are temporally short-lived. Therefore for this purpose, a time-averaged flow-field would be a better representation of a characteristically unsteady flow. The time-averaged flow-field is however shown to be inappropriate for deriving other flow variables such as wall shear stress, but may be used for transport purposes as a convective profile.

Acknowledgments

References

[1] Assemat, P. et al., Three-dimensional numerical simulation of blood flow in mouse aortic arch around atherosclerotic plaques. *Applied Mathematical Modelling*, 2014

[2] Cilla, M., Peña, E. & Martínez, M.A., Mathematical modelling of atheroma plaque formation and development in coronary arteries, *Journal of the Royal Society, Interface*, **11**, 2014, 1-16.

[3] Ethier, C.R., Computational Modeling of Mass Transfer and Links to Atherosclerosis, *Annals of Biomedical Engineering*, **30**, 2002, 461-471.

[4] Gabriel, S.A., Ding, Y., Feng, Y. & Gear, J.A., Deposition-driven growth in atherosclerosis modelling, *19th Australasian Fluid Mechanics Conference*, 2014

[5] Himburg, H.A. et al., Spatial comparison between wall shear stress measures and porcine arterial endothelial permeability, *American journal of physiology. Heart and circulatory physiology*, **286**, 2004, 1916-1922.

[6] Lantz, J., Renner, J. & Karlsson, M., Wall shear stress in a subject specific human aorta - influence of fluid-structure interaction, *International Journal of Applied Mechanics*, **3**, 2011, 759-778.

[7] Liao, W., Lee, T.S. & Low, H.T., Numerical studies of physiological pulsatile flow through constricted tube, *International Journal of Numerical Methods for Heat & Fluid Flow*, **14**, 2004, 689-713.

[8] Liu, X., Fan, Y., Deng, X. & Zhan, F., Effect of non-Newtonian and pulsatile blood flow on mass transport in the human aorta, *Journal of biomechanics*, **44**, 2011, 1123-1131.

[9] Malek, A.M., Alper, S.L. & Izumo, S., Hemodynamic shear stress and its role in atherosclerosis, *JAMA: the journal of the American Medical Association*, 1999, **282**, 2035-2042.

[10] Meyer, G., Merval, R. & Tedgui, A., Effects of pressure-induced stretch and convection on low-density lipoprotein and albumin uptake in the rabbit aortic wall, *Circulation research*, **79**, 1996, 532-540.

[11] Peiffer, V., Sherwin, S.J. & Weinberg, P.D., Does low and oscillatory wall shear stress correlate spatially with early atherosclerosis? A systematic review, *Cardiovascular research*, 2013, **99**, 242-250.

[12] Sakellarios, A.I. et al., Patient-specific computational modeling of subendothelial LDL accumulation in a stenosed right coronary artery: effect of hemodynamic and biological factors, *American journal of physiology. Heart and circulatory physiology*, 2013, **304**, 1455-1470.

[13] Soulis, J.V., Fytanidis, D.K., Papaioannou, V.C. & Giannoglou, G.D., Wall shear stress on LDL accumulation in human RCAs, *Medical engineering & physics*, 2010, **32**, 867-877.

[14] Stangeby, D.K. & Ethier, C.R., Computational analysis of coupled blood-wall arterial LDL transport, *Journal of biomechanical engineering*, **124**, 2002, 1-8.

[15] Younis, H.F. et al., Hemodynamics and wall mechanics in human carotid bifurcation and its consequences for atherogenesis: investigation of inter-individual variation, *Biomechanics and modeling in mechanobiology*, 2004, **3**, 17-32.